IEEE Access
Multidisciplinary | Rapid Review | Open Access Journal

Received 27 June 2023, accepted 9 August 2023, date of publication 14 August 2023, date of current version 18 August 2023.

Digital Object Identifier 10.1109/ACCESS.2023.3304914

RESEARCH ARTICLE

Intelligence Recognition of Clotting Level in Hemodialysis

TIANXIAO WANG[1], QING SHAO[2], RAN LI[1], YIMING LI[1], NANMEI LIU[2], AND HUI YANG[1]
[1]School of Optical-Electrical and Computer Engineering, University of Shanghai for Science and Technology, Shanghai 200093, China
[2]Department of Nephrology, Naval Medical Center of PLA, Shanghai 200052, China

Corresponding authors: Hui Yang (yangh_23@sumhs.edu.cn) and Nanmei Liu (13585996275@163.com)

This work was supported by the Pudong New Area Production-Study-Research Project under Grant PKX2021-D10.

ABSTRACT The consequences of clotting formation during hemodialysis are highly consequential, highlighting the need for a clotting detection technology that offers real-time responsiveness and high accuracy to monitor clotting in the context of hemodialysis. Currently, clotting detection primarily relies on visual observation by medical workers and offline testing following scheduled blood sampling, which falls short in providing real-time insights into clotting status. In this study, we present a clotting detection device based on the MS-UNet++ framework, capable of identifying clotting areas and assessing the clotting levels in real time through venous pot images within the hemodialysis circuit. Clinical experiments have demonstrated that this model achieves an accuracy of 84.0% in classifying the clotting levels. Furthermore, when it comes to alerting for clotting levels exceeding the threshold, the model exhibits a sensitivity of 100%. These results affirm the ability of the MS-UNet++ framework to accurately identify clotting levels during the hemodialysis process and provide timely warnings when necessary. The stability and applicability of the neural network model in clotting detection have been verified, offering novel insights and approaches for real-time clotting monitoring during hemodialysis.

INDEX TERMS Clotting level, MS-UNet++, image segmentation, clotting alarm.

I. INTRODUCTION

Hemodialysis is a common clinical treatment for end-stage renal disease (ESRD) [1], [2], [3], [4]. It involves the purification of blood through an extracorporeal circuit by removing uremic toxins, including small molecules such as urea, creatinine, uric acid, and middle molecules like β2-microglobulin [5], [6], [7], [8], [9], [10]. During hemodialysis, activation of platelets, leukocytes, and the coagulation cascade can lead to clotting formation [11], [12], [13], [14], [15], [16]. The consequences of clotting during hemodialysis are severe. If clotting are limited to the dialyzer fibers without affecting the extracorporeal circulation, the effective surface area of the dialyzer is reduced, impacting treatment efficacy [17]. However, if clotting obstructs blood flow from the dialysis circuit back to the patient, significant blood loss can occur. In severe cases, immediate termination of dialysis is required, posing potential life-threatening risks. Therefore, detecting clotting during hemodialysis is of paramount importance. Medical workers find it challenging to continuously monitor clotting in all patients within the hemodialysis facility, necessitating a clotting detection technique with high real-time responsiveness and accuracy to monitor clotting during the procedure.

Currently, there are two types of clotting detection techniques used in hemodialysis. In 2012, Aniort et al. [18] introduced a method that relies on visual observation of the percentage of dark red stripes on the dialyzer to assess the patient's clotting level after hemodialysis [19]. However, this method can only determine the clotting level of the dialyzer after the completion of hemodialysis, following rinsing with saline solution, and it fails to observe clotting changes during the actual procedure. Moreover, each observation requires the presence of specialized medical workers.In order to assess clotting activation during hemodialysis, François et al. [20] conducted experiments by collecting blood samples at various time points, including before and 5, 15, 30, 90, and 240 minutes after the initiation of the blood pump. In the

The associate editor coordinating the review of this manuscript and approving it for publication was Mingbo Zhao.

study, clotting activation was evaluated based on markers such as thrombin-antithrombin complex (TAT), prothrombin fragment 1+2 (PF1+2), activated factor XII (FXIIa), kallikrein, activated factor XI (FXIa).This approach requires offline laboratory testing and cannot provide real-time monitoring of clotting levels. Therefore, there is a pressing need for an online method to assess clotting levels during hemodialysis.

Image segmentation has become a common approach in medical image processing in recent years, serving as a crucial step for feature extraction and classification during medical analysis. Segmentation refers to the partitioning of an image into multiple categories or regions with shared characteristics, allowing for the extraction of regions of interest in medical applications [21], [22], [23], [24]. In the extracorporeal circulation during hemodialysis, the venous pot images can be captured and analyzed. Due to changes in blood turbidity during the clotting process, noticeable variations occur in the venous pot images, which can be utilized for feature extraction of clotting areas using medical image segmentation methods. Traditional algorithms in medical image segmentation include OTSU, edge detection, and K-means, among others [25], [26]. Although these methods can accomplish simple segmentation tasks, they demonstrate unsatisfactory performance in identifying clotting areas. Therefore, a neural network-based method for medical blood coagulation image segmentation was designed to address this issue.

In recent years, there have been numerous examples in the field of biomedical engineering that utilize deep learning algorithms for image segmentation [27], [28], [29], [30], with the U-Net [31] architecture proving to be highly effective. The U-Net framework is based on Fully Convolutional Network [32]. The U-Net framework achieved an Intersection over Union of 77.5% in microscope cell segmentation tasks. Zhou et al. [33] designed the U-Net++ framework to address the need for more accurate segmentation in medical images. The encoding and decoding subnetworks are interconnected through a series of nested and dense skip connections, achieving an Intersection over Union of 82.9% in liver segmentation tasks and 77.2% in lung nodule segmentation tasks. The U-Net and U-Net++ frameworks have been widely applied in biomedical engineering for segmentation tasks, demonstrating excellent performance while adapting to the scarcity of medical image datasets, requiring minimal data. However, there is still significant room for improvement when it comes to clotting images within this network. Therefore, it is proposed to develop a model based on this framework specifically for medical clotting image segmentation to address the segmentation task, as well as classify the severity based on the clotting area.

The method proposed in this study is capable of assessing clotting levels at various time points during the hemodialysis process, not only at the end of the procedure. It eliminates the need for offline detection after blood sampling and provides alerts when the clotting level exceeds a threshold. The approach has been applied and tested during hemodialysis sessions with different patients, and the experimental results confirm the stability, universality, and scalability of the neural network algorithm in clotting image detection.

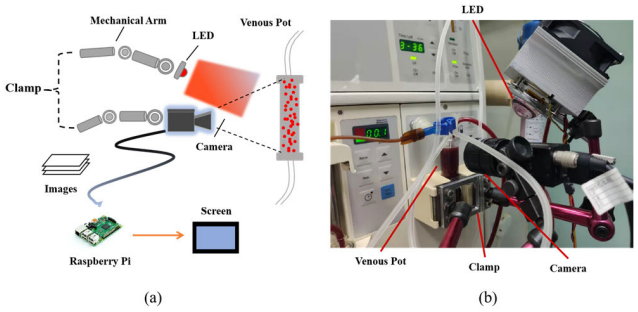

FIGURE 1. The experimental setups of clotting detection: (a) Experimental schematic diagram of the clotting detection. (b) Portable Experimental System.

II. METHODOLOGY

A. EXPERIMENTAL SETUP

The measurement device shown in Fig. 1 (a) was constructed using the following components: near-infrared CMOS camera (1280 × 1024 pixels), near-infrared LED (wavelength: 850 nm, power: 15 W), filter (cut-off wavelength: 850 nm, bandwidth: 50 nm), touch screen (7 inches, 1024 × 600 pixels), embedded system (Raspberry Pi 4 Model B with 8 GB of memory).

In this experiment, the near-infrared LED light source, which provides the light, is positioned directly above the near-infrared CMOS camera to eliminate ambient light interference. The filter is placed in front of the lens of the near-infrared CMOS camera to improve the clarity and accuracy of the imaging results. The captured venous pot images by the near-infrared CMOS camera are stored in the PC and converted into grayscale and pseudo-color images, which are then displayed on the touch screen. The settings input through the touch screen are sent to the PC, which outputs control signals to the near-infrared LED light source. The system is fixed at the clamp of the venous pot and can be adjusted in all directions through a mechanical arm to support the positioning of the LED light source and the CMOS camera.

The apparatus diagram is presented in Fig. 1 (b). The constructed device is initially fixed at the clamp of the venous reservoir. The position of the near-infrared light source and the camera's acquisition position are adjusted using a mechanical arm, followed by the adjustment of the camera's focal length and aperture. The goal is to achieve clear and evenly illuminated images.

Once the device is activated for measurement, the acquisition frequency is set to 30 seconds. Fig. 2 shows the venous pot images obtained at three different time points during hemodialysis. The images have a resolution of 1280 × 1024 pixels. The clotting areas appear darker than the normal blood area and can be visually observed and identified. They may appear at different locations within the venous pot and

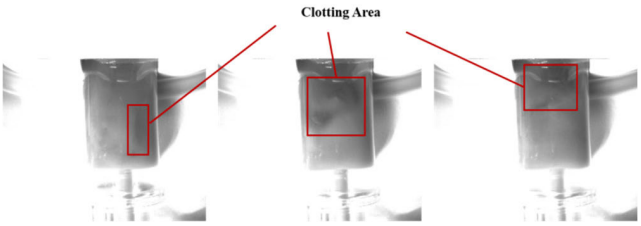

FIGURE 2. The venous pot images at different time points.

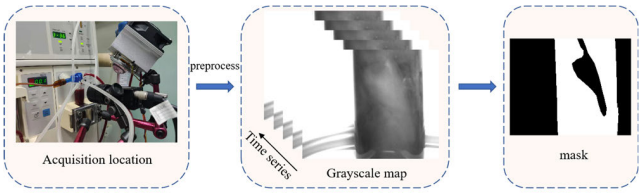

FIGURE 3. The production process of clotting area dataset.

exhibit various shapes. The specific locations of the blood clotting areas in the three images are highlighted with red boxes.

B. DATASET

The present study comprised a cohort of 103 patients diagnosed with ESRD who had been receiving dialysis treatment for a minimum of three months at Naval Medical Center of PLA. All patients are aware of the purpose of image acquisition. The cohort consisted of 53 male and 50 female patients. The dialysis machines employed in the study were the Fresenius 4008B and Fresenius 4008S, with a dialyzer surface area ranging from 1.4-1.8 square meters. The patients underwent three dialysis sessions per week, each session lasting 3.5-4 hours. The blood flow rate ranged from 200 to 260 mL/min, and the dialysate flow rate was set at 500 mL/min. The dialysate contained a sodium concentration of 140 mmol/L and a bicarbonate concentration of 35 mmol/L. The anticoagulation protocol involved administering low-molecular-weight heparin at a dosage of 60-80 U/kg or sodium citrate at a rate of 300-400 mL/h. Patients' exclusion criteria were as follows: patients aged 78 years and above, those with contraindications to heparin, severe liver disease, chronic inflammatory diseases, hematological disorders, vascular dysfunction, or those taking ciprofloxacin, warfarin, or antiplatelet drugs. The patients did not exhibit any distinctive characteristics.

In order to obtain images that reflect clotting in the venous pot, the aforementioned experimental setup was used to capture images of the venous pot throughout the entire process of patients hemodialysis. During the process of hemodialysis, clotting formation and expansion often occur rapidly. The image capture frequency was set to capture an image of the venous pot every 30 seconds, allowing for a complete record of the clotting process in the venous pot. The captured images using the aforementioned setup had a pixel resolution of 1280×1024.

The acquired raw images are preprocessed to enhance their quality. Firstly, the original images are converted to grayscale to reduce the parameter count and facilitate subsequent processing steps. The environmental lighting in the hemodialysis room introduces significant interference in the images, leading to uneven illumination in the venous pot images. This is characterized by non-uniform brightness and color distribution across the entire image. To address this issue, gamma correction is applied as a preprocessing step to adjust the grayscale images [34]. Gamma correction employs a nonlinear transformation to adjust the brightness of the images, enhancing their quality and effectively mitigating the impact of uneven lighting conditions.

Based on the preprocessed images, the pixel points within the clotting area and venous pot area are used to calculate the ratio between these two regions. This ratio is then utilized to determine the level of clotting. To obtain accurate masks for the venous pot area and clotting area, experienced clinical physicians create the dataset masks. The specific process is illustrated in Fig. 3. Medical experts annotating the venous pot images may provide significantly different results in certain cases. Some may classify the same region as normal blood, while others may classify it as a clotting area. The boundaries of the venous pot area are distinct, with a shape resembling a rectangle, similar in size and position. The distinct boundaries make it easier to determine. The mask for the venous pot area is created with reference to the results of traditional algorithms, but with improvements incorporated. On the other hand, the boundaries of the clotting area are not well-defined, and the shape and size can be complex. During hemodialysis, normal blood exhibits flow within the venous pot, while clotting does not. To determine the clotting area, the dataset is created by three professional clinical physicians who compare images from different time points and collectively select the region that best approximates the true area of clotting.

C. MS-UNET++ FRAMEWORK

U-Net is specifically designed to handle small datasets and has been widely applied in medical image segmentation [31]. In the collected venous pot images, the color of the patient's blood varies, resulting in significant differences in grayscale values in the obtained grayscale images. The clotting area appears as an irregular shape with a darker center and lighter color in the surrounding regions, forming at arbitrary positions. The surrounding areas have lighter colors, similar to the color of the surrounding normal blood, and their boundaries are relatively blurred. In the case of clotting images of the venous pot, the U-Net structure tends to perform poorly in capturing the edge information of clotting images due to the significant semantic gap between the feature maps of the encoder and decoder. Zhou et al. proposed the U-Net++ framework, which introduces a series of nested and dense

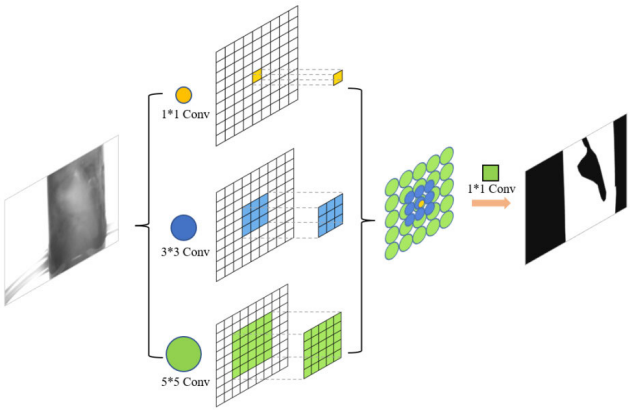

FIGURE 4. Principle of multi-scale convolution.

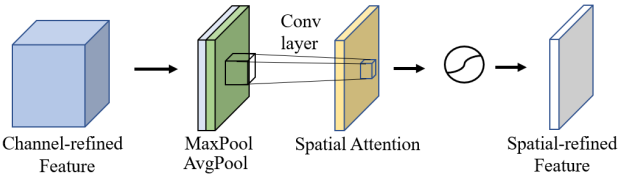

FIGURE 5. Principle of spatial attention mechanism.

convolution blocks along the skip connections of U-Net [33]. The U-Net++ framework reduces the semantic gap between the feature maps of the skip connections and achieves better edge information extraction for clotting image features compared to U-Net. However, the performance of U-Net++ in handling the varied irregular shapes and sizes of the clotting areas is limited. Although U-Net++ utilizes skip connections for feature fusion, there is still room for improvement in extracting edge information for clotting image features during the segmentation process.

To address the uncertainty in the shape and size of clotting areas in input clotting images, a multi-scale convolution is employed to replace the VGG module in the U-Net++ for feature extraction [35]. The multi-scale convolution structure, as shown in Fig. 4, applies convolutional kernels of three different scales to extract feature maps with varying receptive fields in clotting images. The three different feature maps obtained are then interpolated to the same size and resolution, concatenated together to form a complete multi-scale feature map. The multi-scale convolution may generate feature maps with a larger depth. To reduce the number of parameters and computational complexity, 1×1 convolutional kernels are concatenated after obtaining the feature maps to reduce their depth to a smaller dimension. The formula for the entire module is shown in (1).

$$F_{out} = (F_{in} \times K_1 + F_{in} \times K_3 + F_{in} \times K_5) \times K_1 \quad (1)$$

where F_{in} represents the input image, F_{out} represents the output feature map. K_1, K_3, K_5 refer to the convolutional kernels of sizes 1×1, 3×3, and 5×5.

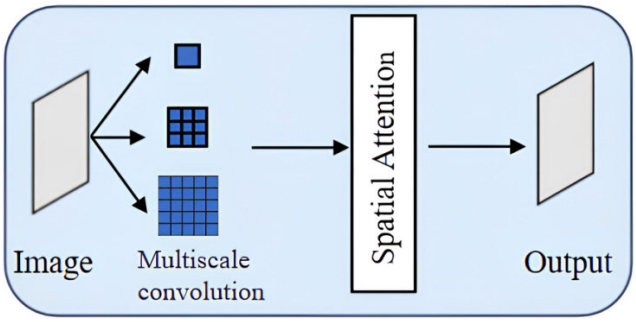

FIGURE 6. Principle of MS module.

To address the challenges of extracting unclear and complex features in clotting images, a spatial attention mechanism is employed to focus on the relevant information in the feature map [36]. The structure of the spatial attention mechanism is illustrated in Fig. 5. After performing convolution, dilated convolution, and convolution operations on the input image, the extracted features are aggregated in the channel dimension using maximum and average pooling. The CxWxH (channel*width*height) feature map is compressed into 1xWxH information. Attention information is then extracted through convolution with attention weights. Finally, if it is a single-branch structure, a sigmoid function is applied to ensure non-negative attention weights. For multi-branch structures, softmax is used to ensure non-negative attention weights. The formula for the spatial attention mechanism is shown in (2).

$$M_S(F) = \sigma(f^{7\times7}([AvgPool(F), MaxPool(F)])) \quad (2)$$

Based on the multi-scale convolution and spatial attention mechanism, an MS module is designed to address the segmentation problem of irregular and complex clotting areas. The structure of the MS module is depicted in Fig. 6, where the spatial attention mechanism module is connected after the multi-scale convolution. The image is initially processed with three different scales of convolution kernels to obtain three distinct feature maps. These feature maps are then concatenated to form a complete multi-scale feature map, which is further dimensionally reduced using a 1×1 convolution kernel. The spatial attention mechanism is subsequently applied to extract relevant positional information.

The MS module is introduced into the U-Net++ framework, resulting in the proposed MS-UNet++ framework. This structure is more suitable for complex and irregular clotting areas. Fig. 7 illustrates the MS-UNet++ framework along with the input and output of feature region recognition. The clotting image data is input to the MS module at X0,0, and the resulting feature map is passed through downsampling and skip connections to enter the next MS module. L1 to L4 represent the network structures after 1 to 4 downsampling and upsampling operations. The final feature map is obtained through a series of encoding and decoding processes and is output from X0,4. In the MS-UNet++ structure,

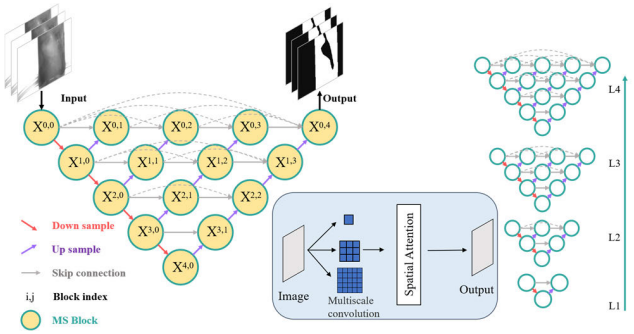

FIGURE 7. Principle of MS-UNet++.

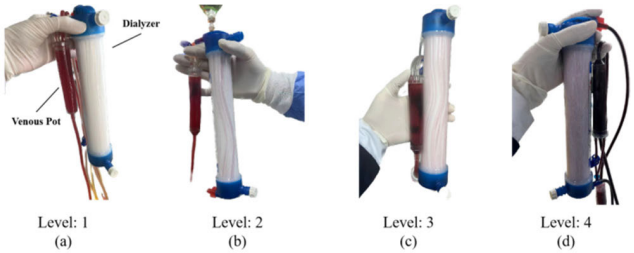

FIGURE 8. Experimental results of comparison between dialyzer and venous pot: (a) First-degree clotting level. (b) Second-degree clotting level. (c) Third-degree clotting level. (d) Fourth-degree clotting level.

downsampling is performed using a 2 × 2 Max Pooling Layer, upsampling is performed using a 2 × 2 Deconvolution Layer, and feature map concatenation is achieved using merge layers.

D. EVALUATION INDEX

Julien et al. first introduced the percentage of dark red stripes in the post-flush dialyzer as a medical evaluation indicator for clotting in hemodialysis [18]. In order to investigate the correlation between clotting in the venous pot and clotting in the dialyzer, a medical standard experiment was conducted to compare the degree of clotting in the venous pot and the dialyzer. The proportion of dark red stripes in the dialyzer to the total dialyzer was used as the clotting level for the dialyzer, while the proportion of clotting in the venous pot to the venous pot was used as the clotting level for the venous pot.

Fig. 8(a)-(d) depict a comparative analysis of clotting areas in the venous pot and the dialyzer for four clotting levels. The dark red clots in the venous pot represent areas of clotting, while the dark red stripes in the dialyzer indicate areas of clotting. In Fig. 8 (a), both the dialyzer and the venous pot show clotting percentages less than 10%, indicating a first-degree clotting level. In Fig. 8 (b), the clotting percentages in both the dialyzer and the venous pot range from 10% to 25%, representing a second-degree clotting level. In Fig. 8 (c), the clotting percentages in both the dialyzer and the venous pot range from 25% to 50%, indicating a third-degree clotting level. Lastly, in Fig. 8 (d), the clotting percentages in both the dialyzer and the venous pot exceed 50%, indicating a fourth-degree clotting level.

TABLE 1. Clotting scale.

Clotting level	Clotting ratio
1	Clotting in less than 10%
2	Clotting 10%-25%
3	Clotting 25%-50%
4	Clotting >50%

Medical standard experiments have demonstrated a high correlation between clotting levels in the dialyzer and the venous pot. Recognizing the extent of clotting in the venous pot can effectively reflect the degree of clotting in the dialyzer. The percentage of clotting areas in the venous pot relative to its total area can also serve as an evaluation indicator for clotting during hemodialysis. The four levels of medical clotting evaluation criteria are shown in Table 1.

In the feature extraction results of the venous pot area and the clotting area, we aim to analyze the accuracy of the segmentation obtained by the model. Additionally, we intend to classify the segmented images into different levels based on the area method and evaluate the final classification accuracy.

In the evaluation of venous pot segmentation and clotting area segmentation performance, for each image, the ground truth mask and the predicted mask are compared, and the pixels of the two masks are determined. Then, the following two metrics are used to evaluate the image segmentation: Dice Similarity Coefficient (DSC) and Intersection over Union (IoU). These metrics are defined by the following equations:

$$DSC = \frac{2TP}{2TP + FP + FN} \tag{3}$$

$$IoU = \frac{TP}{TP + FP + FN} \tag{4}$$

In this context, TP represents the number of pixels correctly classified by the model as clotting areas, FP represents the number of pixels mistakenly classified by the model as clotting areas when they are not, and FN represents the number of pixels that were not classified as clotting areas but actually belong to clotting areas.

DSC, also known as the F1 score or F-measure, and IoU, sometimes referred to as the Jaccard index, are two evaluation metrics used in image segmentation. DSC measures the overlap between the predicted segmentation and the ground truth segmentation, emphasizing the similarity between the two. On the other hand, IoU calculates the ratio of intersection to union, focusing on the consistency between the predicted and ground truth segmentations. DSC provides a stricter evaluation of the segmentation results, while IoU tends to prioritize the consistency between the predicted and ground truth results. Both metrics are commonly used in medical image segmentation tasks. A higher value of DSC and IoU, closer to 1, indicates a smaller difference between the extracted results and the labels, indicating higher accuracy. Conversely,

a value closer to 0 indicates a larger difference and poorer performance of the segmentation results.

For the segmented images, the number of pixels in the venous area and the clotting area are calculated separately. The pixel counts are compared using the area method to determine the clotting level, which is categorized into four classes. The performance of the model's classification is evaluated using the Accuracy, Macro-Precision, and Macro-Recall metrics, defined by the following equations:

$$\text{Accuracy} = \frac{TP_1 + TP_2 + TP_3 + TP_4}{ALL} \tag{5}$$

$$\text{Precision} = \frac{TP}{TP + FP} \tag{6}$$

$$\text{Recall} = \frac{TP}{TP + FN} \tag{7}$$

$$\text{Macro-Precision} = \frac{P_1 + P_2 + P_3 + P_4}{4} \tag{8}$$

$$\text{Macro-Recall} = \frac{R_1 + R_2 + R_3 + R_4}{4} \tag{9}$$

The Accuracy metric measures the overall prediction performance on the entire dataset. To address data imbalance, Precision and Recall are introduced for evaluation. For multi-class tasks, Precision and Recall need to be calculated separately for each class, and then averaged using the Macro-average method. TP_1, TP_2, TP_3 and TP_4 represent the number of correctly classified samples in the four classes of clotting. ALL represents the total number of samples. P_1, P_2, P_3, and P_4 represent the Precision of each individual category, while R_1, R_2, R_3, and R_4 represent the Recall of each individual category. The values of Accuracy, Macro-Precision, and Macro-Recall closer to 1 indicate smaller differences between predicted and true results, indicating higher accuracy. Values closer to 0 indicate larger differences between predicted and true results, indicating lower accuracy.

Based on the evaluation metrics of neural networks, the performance of the classification task is analyzed to assess the accuracy of the neural network model in classifying the degree of clotting. The evaluation is conducted using metrics such as Accuracy, Macro-Precision, and Macro-Recall. By comparing the metrics obtained from the neural network with the actual clotting levels assessed by medical evaluation metrics, the accuracy of the classification task can be determined. The accuracy of the classification obtained from this model can be used to evaluate the accuracy of the clotting level in medical evaluation metrics during hemodialysis.

For clinical applications, it is crucial to determine whether clotting has occurred and issue appropriate alarms. The accuracy of clotting detection is assessed using Sensitivity and Specificity measures. They are defined by the following equations:

$$\text{Sensitivity} = \frac{TP}{TP + FN} \tag{10}$$

$$\text{Specificity} = \frac{TN}{TN + FP} \tag{11}$$

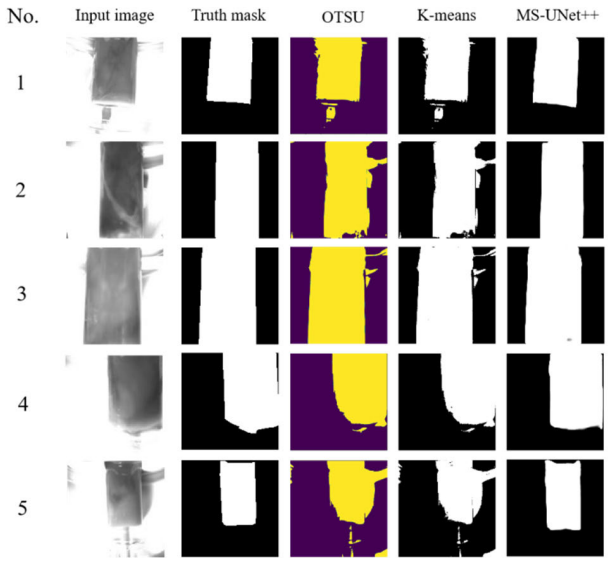

FIGURE 9. Segmentation results of the venous pot. Results of K-means algorithm and MS-UNet++ algorithm for venous pot segmentation: In the obtained results, the white regions represent the venous pot, while the black regions correspond to the background.The yellow regions is used for a more pronounced contrast between the segmentation results of OTSU and K-means.

Sensitivity refers to the proportion of true positive cases correctly identified among all individuals who actually have the condition, indicating the true positive rate. Specificity, on the other hand, refers to the proportion of true negative cases correctly identified among all individuals who do not have the condition, indicating the true negative rate. Sensitivity and Specificity are complementary measures that are often considered together. A higher value for Sensitivity and Specificity indicates a smaller discrepancy between the extracted results and the labels, resulting in higher accuracy. Conversely, a lower value indicates a larger discrepancy and poorer performance.

III. EXPERIMENTAL RESULTS AND DISCUSSION

A. SEGMENTATION OF THE VENOUS POT AREA

Accurately segmenting the size of the venous pot is essential for subsequent calculation of clotting levels using the area method. By comparing the segmentation results of the venous pot using traditional image segmentation algorithms with the MS-UNet++ framework, different regions of the venous pot were obtained as shown in Fig. 9. It demonstrates the venous pot segmentation results of five different images using the OTSU method, K-means method, and MS-UNet++. From the obtained venous pot segmentation results, it can be observed that using neural networks for venous pot segmentation yields results that are closer to the true venous pot mask compared to traditional methods. It effectively removes interference from shadows in the background and dialysis tubing, accurately locating the true region of the venous pot.

The adoption of the traditional image segmentation algorithm, namely the OTSU algorithm, enables automatic

TABLE 2. Performance of different algorithm in segmenting the venous pot area.

Algorithm	DSC	IOU
OTSU	0.7276	0.7564
K-means	0.7234	0.7556
MS UNet++	0.9763	0.9842

selection of an appropriate threshold for binary segmentation of grayscale images [25]. The image segmentation algorithm based on K-means clustering, with the number of cluster centers set to 2, can automatically segment the venous pot area [26]. These two traditional algorithms can generate an approximate image of the venous pot. However, due to uneven lighting conditions in the hemodialysis room, the background of the obtained grayscale image is prone to shadow areas. The dialysis tubing itself consists of many elongated tubes, which are likely to appear in the background and are difficult to avoid in practical clinical settings. Although this portion shares the same color as the venous pot, it is not within the range we need to calculate. The traditional OTSU algorithm and K-means clustering algorithm perform poorly in recognizing shadows and dialysis tubing during venous pot segmentation, often mistakenly identifying them as part of the venous pot. In contrast, MS-UNet++ addresses this issue.

The 50 test images from data1 were segmented using three different methods and compared with the ground truth masks. The obtained IoU coefficients are presented in Table 2. With the increase in training epochs, the MS-UNet++ framework achieved the highest IoU coefficient of 98.4% on the test set and a DSC of 97.36%, outperforming traditional algorithms. This validates the suitability of the neural network model for venous chamber segmentation tasks.

B. SEGMENTATION OF THE CLOTTING AREA

The differences in clotting areas and other blood regions within the venous pot are minimal, making it challenging for traditional methods such as binarization and clustering to segment the clotting areas accurately. To address this limitation and overcome the inability of traditional algorithms to segment the clotting areas, three neural network models were employed to perform segmentation tests on data1 in order to find the optimal weights.

Fig. 10 shows the comparison of IoU and DSC of three network models as training progresses. It can be observed that with increasing training iterations, both the IoU and DSC of MS-Unet++ outperform those of U-Net and U-Net++. Table 3 presents the optimal values obtained within 100 epochs, where the DSC of MS-UNet++ reaches 83.25% and the IoU coefficient reaches 84.35%, indicating higher segmentation accuracy compared to the U-Net and U-Net++.

The boundary between flowing blood and the clotting area exhibits minimal differences, making it challenging for the

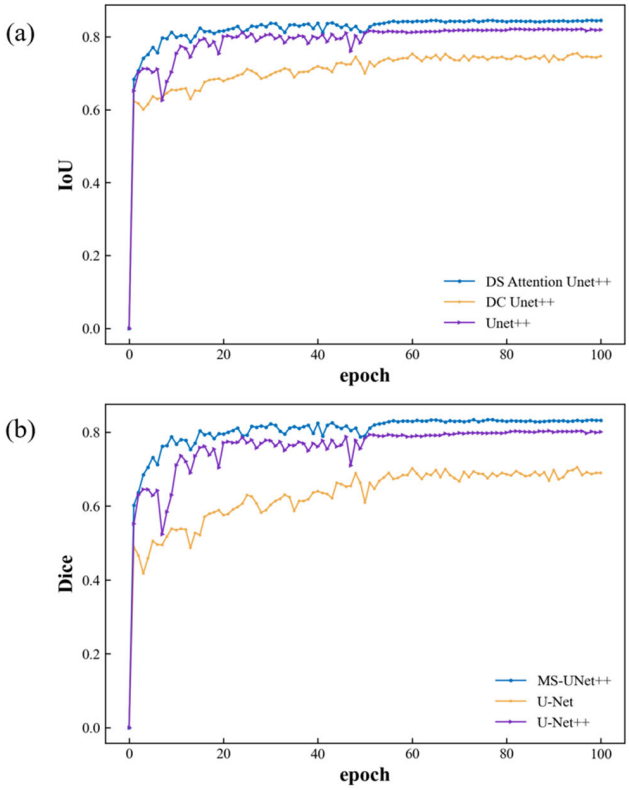

FIGURE 10. The change of DSC and IoU with the epoch.

TABLE 3. Performance of different framework in segmenting the clotting area.

Framework	DSC	IOU
U-Net	0.7012	0.7513
U-Net++	0.8008	0.8234
MS-UNet++	0.8325	0.8435

U-Net and U-Net++ to effectively handle this edge information. Moreover, these models struggle to accurately identify the irregular shapes of the clotting areas. In contrast, the improved algorithm of the MS-UNet++ framework, specifically designed for segmenting clotting areas, enhances the perception capability for these areas and enables better capture of edge information within the images.

Fig. 11 illustrates partial results of image segmentation using MS-UNet++. Five images with different positions and shapes were selected from the test dataset. The combined image highlights the following areas: white for predicted and actual clotting areas, green for predicted clotting but actual non-clotting areas, black for predicted and actual non-clotting areas, and purple for predicted non-clotting but actual clotting areas. It is evident from the combined images that MS-UNet++ accurately identifies the locations of clotting areas and effectively handles edge information. Even in cases where the clotting areas closely resemble the background color, the framework successfully delineates the boundaries

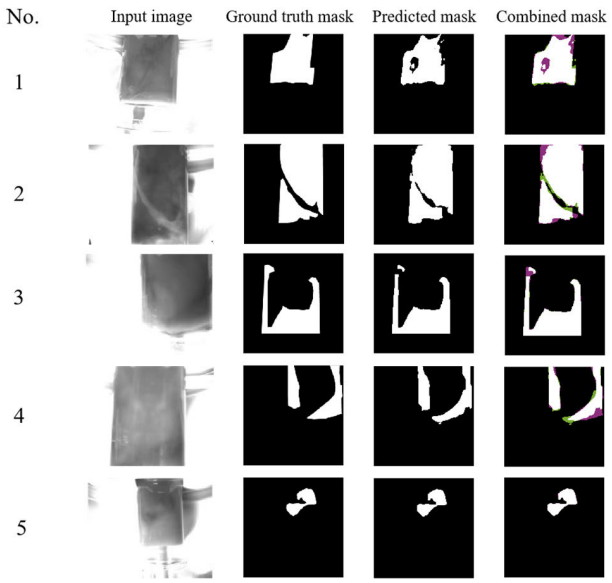

FIGURE 11. Segmentation results of the clotting area. The combined image highlights the following areas: white for predicted and actual clotting areas, green for predicted clotting but actual non-clotting areas, black for predicted and actual non-clotting areas, and purple for predicted non-clotting but actual clotting areas.

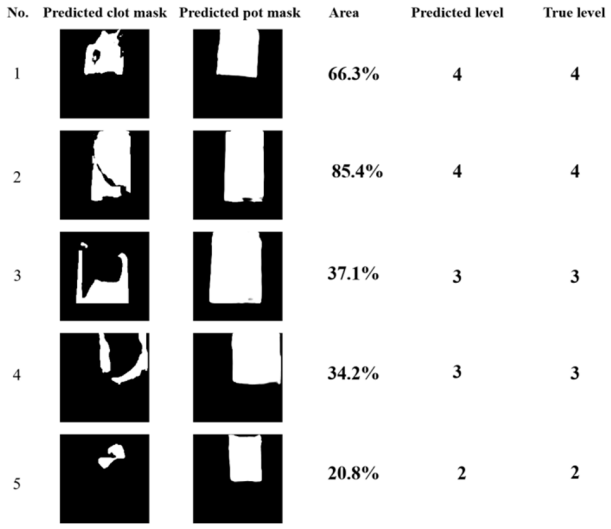

FIGURE 12. Classification results of the clotting images.

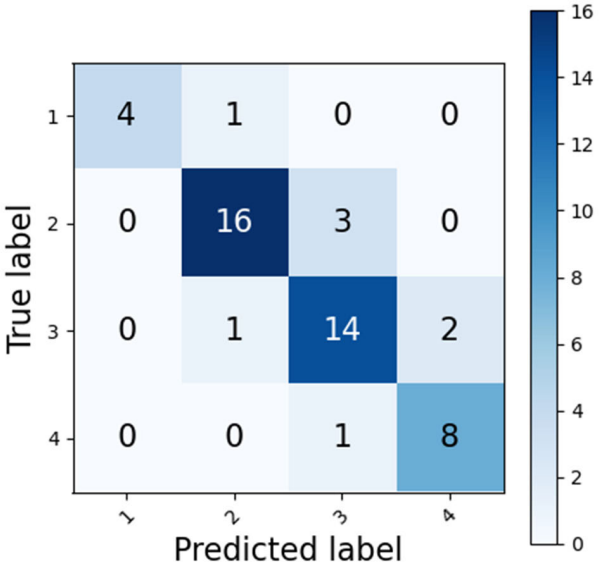

FIGURE 13. Confusion matrices for classifying data1.

of the clotting areas. These results validate the improved performance of MS-UNet++ in clotting area segmentation.

C. CLASSIFICATION OF CLOTTING

The above experiments resulted in the predicted masks for the venous pot and the clotting area using the model. First, it is determined that the mask of the clotting area should be contained within the venous pot mask. Therefore, the masks of the clotting area that are not within the venous pot mask are removed. The pixel count of the clotting area mask and the venous pot mask is then calculated to obtain their respective areas. These areas are divided into four categories based on the ratio between them. The first-degree clotting level represents 0-10%, the second-degree clotting level represents 10-25%, the third-degree clotting level represents 25-50%, and the fourth-degree clotting level represents 50-100%.

The partial results of data classification are shown in Fig. 12. The ''Area'' represents the proportion of the clotting area, ''Predicted Level'' indicates the predicted level, and ''True Level'' represents the actual clotting level. No. 1 and No. 2 belong to the fourth-degree clotting level, No. 3 and No. 4 belong to the third-degree clotting level, and No. 5 belongs to the second-degree clotting level. All five images can be accurately classified into their corresponding levels. Even if there are errors in segmenting the clotting area, there are instances where accurate classification into the corresponding level is still possible during level classification, thereby reducing the impact of segmentation errors.

Fig. 13 shows the confusion matrix of the 50 clotting images classified from the automatically randomized test set. Level 2 and Level 3 data are more abundant compared to Level 1 and Level 4. Based on the confusion matrix, various evaluation metrics are calculated. The results show Accuracy of 84.0%, Macro-precision of 86.7%, and Macro-recall of 83.8%. All metrics achieve precision exceeding 80%, demonstrating the model's good performance in the classification task and its effectiveness in the four-class classification. The higher macro-precision than accuracy and the slightly lower macro-recall compared to accuracy indicate a certain data imbalance issue, especially with the abundance of Level 2 and Level 3. However, the overall model's classification accuracy remains reliable.

To verify the generalization capability of the model, the trained model was used to classify the clotting levels in data2. The resulting confusion matrix is shown in Figure 14. The evaluation metrics were computed as follows: Accuracy =

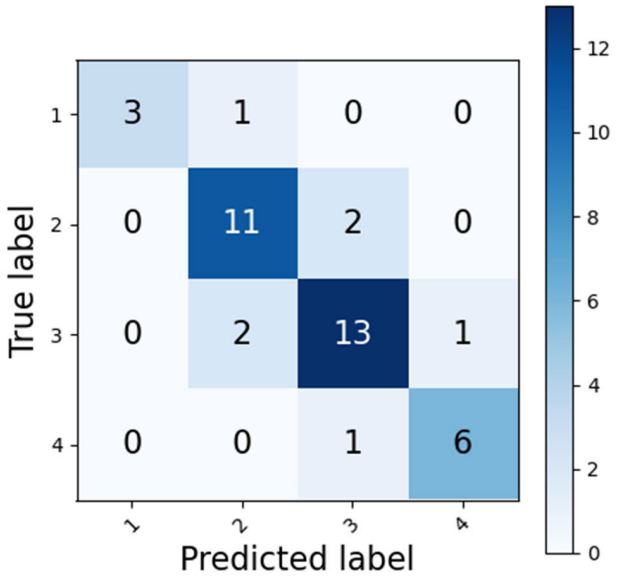

FIGURE 14. Confusion matrices for classifying data2.

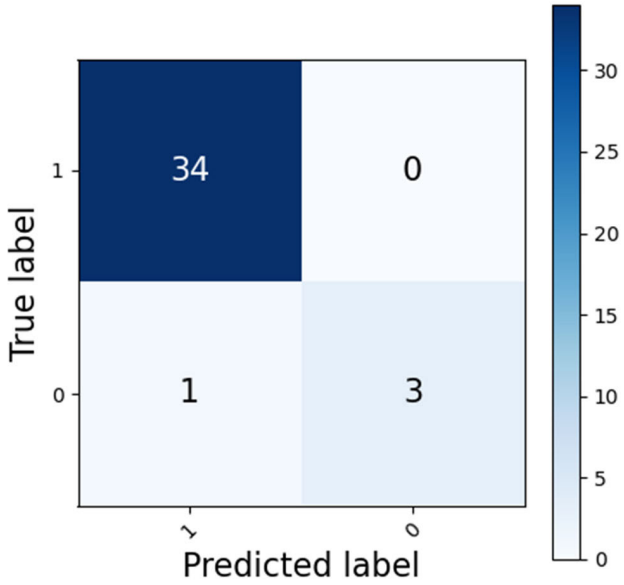

FIGURE 15. Confusion matrices for classifying data2 to two class.

86.8%, Macro-Precision = 87.8%, and Macro-Recall = 82.9%. Data2 still contains a larger proportion of Level 2 and Level 3 samples. The higher macro-precision than accuracy and the slightly lower macro-recall compared to accuracy indicate the presence of data imbalance. However, the overall classification accuracy of the model remains reliable. When facing entirely new data, the model demonstrates consistent or even improved performance, indicating its generalization capability across different datasets.

D. CLOTTING THRESHOLD SETTING AND ALARM

In the clinical application of hemodialysis, the ability to detect and alert the occurrence of clotting is of paramount importance. Researchers define clotting with a level higher than 2 and an area larger than 10% as significant clotting,

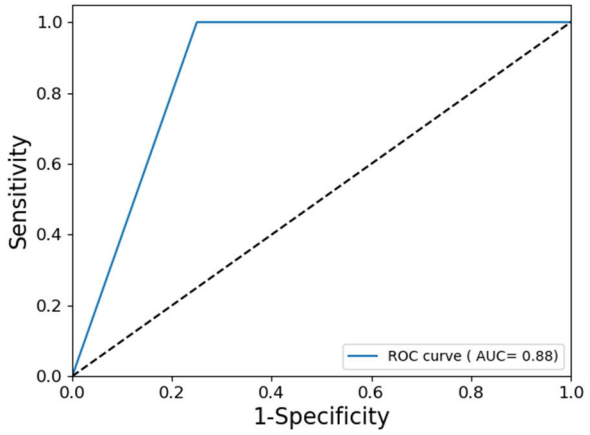

FIGURE 16. ROC curve of clotting alarm.

which often requires early termination of dialysis to avoid potential harm. Clotting that occurs during the hemodialysis process is irreversible, and it is clinically recognized that any clotting of level 2 or higher within 180 minutes after the start of dialysis should trigger an alarm. This alarm alerts healthcare professionals to perform real-time interventions such as saline flushing or additional anticoagulant administration to prevent further enlargement of the clotting area. Failure to intervene may lead to the development of level 4 clotting, necessitating early termination of dialysis.Therefore, clotting records are classified as follows: 0 for level 1 clotting and no clotting, indicating no action required; 1 for levels 2, 3, and 4 clotting, indicating the need for an alarm to alert healthcare workers for intervention. By applying a threshold of 10% clotting area, the results obtained from data2 are divided into two classes. The resulting confusion matrix is shown in Fig. 15, and the accuracy is calculated as 97.3%. However, there is a significant class imbalance in the data, which can be addressed by calculating sensitivity and specificity. The ROC curve in Fig. 16 demonstrates a sensitivity of 100%, specificity of 75%, and an area under the curve of 88%. In this task, considering the potential harm caused by clotting, it is crucial not to miss any clotting cases. Therefore, identifying the proportion of true clotting cases that are successfully detected is of greater importance, emphasizing the significance of sensitivity. In this case, the sensitivity is 100%, confirming the reliability of the model in clotting detection.

IV. CONCLUSION

This study introduces a novel approach to classify the clotting level during hemodialysis directly based on the grayscale images of the venous pot. Regarding the segmentation task, MS-UNet++ demonstrates significant improvements over traditional image segmentation algorithms. It effectively eliminates interferences such as shadows and blood vessels, resulting in more accurate segmentation of the venous pot area. The accuracy of segmentation has been increased from 75% with traditional algorithms to 98% with MS-UNet++.

When comparing the two U-Net architectures with MS-UNet++, it is observed that the latter performs well even with small batch data, particularly in handling irregular and varying shapes of clotting areas. The best DSC on the test set has been improved to 83.25%. Regarding the classification of clotting levels, the model achieves an accuracy of 84.0% based on the area-based classification method. Considering the data imbalance, the model is evaluated comprehensively achieving a Macro-Precision of 86.7%. On data2, the model maintains a high level of accuracy without significant decrease. The reliable classification accuracy and high generalization capability of the model enable it to adapt to new data effectively.

For medical clinical applications, using a threshold of 10% clotting area, the model achieves an accuracy of 97.3% based on the confusion matrix and ROC curve analysis. The sensitivity is 100%, specificity is 75%, and the AUC is 88%. These results confirm that the model can accurately identify clotting occurrences during hemodialysis and trigger alarms. This significantly reduces the risk of blood loss and premature termination of dialysis, thereby alleviating the workload and pressure on healthcare professionals in the hemodialysis department. The findings have significant practical implications in clinical settings.

This study offers a new method and approach for real-time clotting detection during hemodialysis, thereby providing valuable assistance in medical research.

ACKNOWLEDGMENT

(Tianxiao Wang and Qing Shao contributed equally to this work.)

REFERENCES

[1] A. Mollahosseini, A. Abdelrasoul, and A. Shoker, "A critical review of recent advances in hemodialysis membranes hemocompatibility and guidelines for future development," *Mater. Chem. Phys.*, vol. 248, Jul. 2020, Art. no. 122911.

[2] U. Eduok, A. Abdelrasoul, A. Shoker, and H. Doan, "Recent developments, current challenges and future perspectives on cellulosic hemodialysis membranes for highly efficient clearance of uremic toxins," *Mater. Today Commun.*, vol. 27, Jun. 2021, Art. no. 102183.

[3] T. Liyanage, T. Ninomiya, V. Jha, B. Neal, H. M. Patrice, I. Okpechi, M.-H. Zhao, J. Lv, A. X. Garg, J. Knight, A. Rodgers, M. Gallagher, S. Kotwal, A. Cass, and V. Perkovic, "Worldwide access to treatment for end-stage kidney disease: A systematic review," *Lancet*, vol. 385, no. 9981, pp. 1975–1982, May 2015.

[4] D. C. H. Harris et al., "Working groups of the international society of nephrology's 2nd global kidney health summit: Increasing access to integrated ESKD care as part of universal health coverage," *Kidney Int.*, vol. 95, no. 4S, pp. S1–S33, 2019.

[5] H. D. Humes, W. H. Fissell, and K. Tiranathanagul, "The future of hemodialysis membranes," *Kidney Int.*, vol. 69, no. 7, pp. 1115–1119, Apr. 2006.

[6] A. Alonso, J. Lau, and B. L. Jaber, "Biocompatible hemodialysis membranes for acute renal failure," *Cochrane Database Systematic Rev.*, vol. 2010, no. 1, Jan. 2008.

[7] A. F. Ismail et al., "Hemodialysis membrane for blood purification process," in *Membrane Separation Principles and Applications*. Amsterdam, The Netherlands: Elsevier, 2019, pp. 283–314.

[8] O. E. M. T. Beek, D. Pavlenko, and D. Stamatialis, "Hollow fiber membranes for long-term hemodialysis based on polyethersulfone-SlipSkin polymer blends," *J. Membrane Sci.*, vol. 604, Jun. 2020, Art. no. 118068.

[9] S. K. Verma, A. Modi, A. K. Singh, R. Teotia, and J. Bellare, "Improved hemodialysis with hemocompatible polyethersulfone hollow fiber membranes: In vitro performance," *J. Biomed. Mater. Res. B, Appl. Biomaterials*, vol. 106, no. 3, pp. 1286–1298, Apr. 2018.

[10] M. K. van Gelder, J. A. W. Jong, L. Folkertsma, Y. Guo, C. Blüchel, M. C. Verhaar, M. Odijk, C. F. Van Nostrum, W. E. Hennink, and K. G. F. Gerritsen, "Urea removal strategies for dialysate regeneration in a wearable artificial kidney," *Biomaterials*, vol. 234, Mar. 2020, Art. no. 119735.

[11] D. Verbeelen, K. Jochmans, A. G. Herman, P. Van der Niepen, J. Sennesael, and M. De Waele, "Evaluation of platelets and hemostasis during hemodialysis with six different membranes," *Nephron*, vol. 59, no. 4, pp. 567–572, 1991.

[12] G. Pertosa, G. Grandaliano, L. Gesualdo, and F. P. Schena, "Clinical relevance of cytokine production in hemodialysis," *Kidney Int.*, vol. 58, pp. S104–S111, Aug. 2000.

[13] R. Nakazawa et al., "Evaluation of blood coagulation-fibrinolysis system in patients receiving chronic hemodialysis," *Nephron*, vol. 73, no. 3, pp. 407–412, 1996.

[14] K. N. Ekdahl, I. Soveri, J. Hilborn, B. Fellström, and B. Nilsson, "Cardiovascular disease in haemodialysis: Role of the intravascular innate immune system," *Nature Rev. Nephrol.*, vol. 13, no. 5, pp. 285–296, May 2017.

[15] Y. Koga, H. Fujieda, H. Meguro, Y. Ueno, T. Aoki, K. Miwa, and M. Kainoh, "Biocompatibility of polysulfone hemodialysis membranes and its mechanisms: Involvement of fibrinogen and its integrin receptors in activation of platelets and neutrophils," *Artif. Organs*, vol. 42, no. 9, pp. E246–E258, Sep. 2018.

[16] V. Liakopoulos, A. Jeron, A. Shah, D. Bruder, P. R. Mertens, and X. Gorny, "Hemodialysis-related changes in phenotypical features of monocytes," *Sci. Rep.*, vol. 8, no. 1, p. 13964, Sep. 2018.

[17] European Renal Association, "Chronic intermittent haemodialysis and prevention of clotting in the extracorporeal system," *Nephrol Dial Transplant*, vol. 17, no. 7, pp. 63–71, 2002.

[18] J. Aniort, T. Petitclerc, and C. Créput, "Safe use of citric acid-based dialysate and heparin removal in postdilution online hemodiafiltration," *Blood Purification*, vol. 34, nos. 3–4, pp. 336–343, 2012.

[19] T. Trakarnvanich, S. Thirathanakul, N. Sriphueng, P. Thumrongthongjaroon, S. Kurathong, T. Ngamvichchukorn, and T. Trakarnvanich, "The effect of citrate on clot formation, dialyzer reuse, and anemia in hemodialysis patients," *Blood Purification*, vol. 47, no. 4, pp. 361–368, 2019.

[20] K. François, C. Orlando, K. Jochmans, W. Cools, V. De Meyer, C. Tielemans, and K. M. Wissing, "Hemodialysis does not induce detectable activation of the contact system of coagulation," *Kidney Int. Rep.*, vol. 5, no. 6, pp. 831–838, Jun. 2020.

[21] H. Zhang, J. E. Fritts, and S. A. Goldman, "Image segmentation evaluation: A survey of unsupervised methods," *Comput. Vis. Image Understand.*, vol. 110, no. 2, pp. 260–280, May 2008.

[22] Z. Ma, J. M. R. S. Tavares, and R. M. N. Jorge, "A review on the current segmentation algorithms for medical images," in *Proc. 1st Int. Conf. IMAGAPP*, vol. 1, 2009, pp. 135–140.

[23] W.-X. Kang, Q.-Q. Yang, and R.-P. Liang, "The comparative research on image segmentation algorithms," in *Proc. 1st Int. Workshop Educ. Technol. Comput. Sci.*, vol. 2, 2009, pp. 703–707.

[24] Y. Xia, S. Eberl, L. Wen, M. Fulham, and D. D. Feng, "Dual-modality brain PET-CT image segmentation based on adaptive use of functional and anatomical information," *Computerized Med. Imag. Graph.*, vol. 36, no. 1, pp. 47–53, Jan. 2012.

[25] T. Y. Goh, S. N. Basah, H. Yazid, M. J. A. Safar, and F. S. A. Saad, "Performance analysis of image thresholding: Otsu technique," *Measurement*, vol. 114, pp. 298–307, Jan. 2018.

[26] A. Jose, S. Ravi, and M. Sambath, "Brain tumor segmentation using k-means clustering and fuzzy c-means algorithms and its area calculation," *Int. J. Innov. Res. Comput. Commun. Eng.*, vol. 2, no. 3, 2014.

[27] L.-C. Chen, Y. Zhu, G. Papandreou, F. Schroff, and H. Adam, "Encoder-decoder with atrous separable convolution for semantic image segmentation," in *Proc. Eur. Conf. Comput. Vis. (ECCV)*, 2018, pp. 801–818.

[28] V. Badrinarayanan, A. Kendall, and R. Cipolla, "SegNet: A deep convolutional encoder-decoder architecture for image segmentation," *IEEE Trans. Pattern Anal. Mach. Intell.*, vol. 39, no. 12, pp. 2481–2495, Dec. 2017.

[29] G. Lin, A. Milan, C. Shen, and I. Reid, "RefineNet: Multi-path refinement networks for high-resolution semantic segmentation," in *Proc. IEEE Conf. Comput. Vis. Pattern Recognit. (CVPR)*, Jul. 2017, pp. 5168–5177.

[30] H. Zhao, J. Shi, X. Qi, X. Wang, and J. Jia, "Pyramid scene parsing network," in *Proc. IEEE Conf. Comput. Vis. Pattern Recognit. (CVPR)*, Jul. 2017, pp. 6230–6239.
[31] O. Ronneberger, P. Fischer, and T. Brox, "U-Net: Convolutional networks for biomedical image segmentation," in *Proc. 18th Int. Conf. Med. Image Comput. Comput.-Assist. Intervent. (MICCAI)*, Munich, Germany. Cham, Switzerland: Springer, Oct. 2015, pp. 234–241.
[32] J. Long, E. Shelhamer, and T. Darrell, "Fully convolutional networks for semantic segmentation," in *Proc. IEEE Conf. Comput. Vis. Pattern Recognit. (CVPR)*, Jun. 2015, pp. 3431–3440.
[33] Z. Zhou, M. M. R. Siddiquee, N. Tajbakhsh, and J. Liang, "UNet++: Redesigning skip connections to exploit multiscale features in image segmentation," *IEEE Trans. Med. Imag.*, vol. 39, no. 6, pp. 1856–1867, Jun. 2020.
[34] P. Babakhani and P. Zarei, "Automatic gamma correction based on average of brightness," *Adv. Comput. Sci., Int. J.*, vol. 4, no. 6, pp. 156–159, 2015.
[35] S. Liu and D. Huang, "Receptive field block net for accurate and fast object detection," in *Proc. Eur. Conf. Comput. Vis. (ECCV)*, 2018, pp. 385–400.
[36] S. Woo, J. Park, J. Y. Lee, and I. S. Kweon, "CBAM: Convolutional block attention module," in *Proc. Eur. Conf. Comput. Vis. (ECCV)*, 2018, pp. 3–19.

TIANXIAO WANG received the B.S. degree from the Nanjing Institute of Technology, in 2017. He is currently pursuing the M.S. degree with the University of Shanghai for science and Technology. His research interest includes biomedical imaging.

QING SHAO received the master's degree from the Hubei University of Chinese Medicine, in 2015. In 2015, she joined the Naval Medical Center of PLA, Second Military Medical University. Her research interests include peritoneal dialysis, hemodialysis, and various acute complications of ESRD.

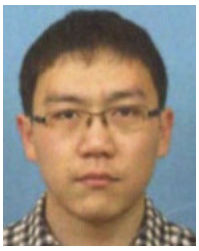

RAN LI received the bachelor's degree in communication engineering from Henan Normal University, in 2012, and the Ph.D. degree in optical engineering from the University of Shanghai for Science and Technology (USST), in 2019. Since July 2019, he has been a Postdoctoral Fellow in biomedical engineering with USST. His research interests include high precision optical measurement and granular matter.

YIMING LI is currently pursuing the Ph.D. degree in control science and engineering with the University of Shanghai for Science and Technology (USST). His research interests include deep learning, photoelectric detection technology, and digital image processing.

NANMEI LIU received the M.D. degree in nephrology from Naval Medical University, in 2014. She is currently a Physician specializing in kidney disease with the Naval Medical Center of PLA. Her research interests include pathogenesis and treatment of acute kidney injury, the improvement of hemodialysis machine, and multidisciplinary applications of blood purification.

HUI YANG received the Ph.D. degree in optical engineering from the University of Shanghai for Science and Technology (USST), in 2009. In 2009, he joined the School of Optical-Electrical and Computer Engineering, USST. His research interests include particle technology, photoelectric precision detection, and digital image processing.